energies

MDPI

Article

LVRT and Reactive Power/Voltage Support of Utility-Scale PV Power Plants during Disturbance Conditions

Omar Alrumayh [1], Khairy Sayed [2] and Abdulaziz Almutairi [3,*]

[1] Department of Electrical Engineering, College of Engineering, Qassim University, Unaizah 56452, Saudi Arabia
[2] Electrical Engineering Department, Faculty of Engineering, Sohag University, Sohag 82524, Egypt
[3] Department of Electrical Engineering, College of Engineering, Majmaah University, Almajmaah 11952, Saudi Arabia
* Correspondence: ad.almutiri@mu.edu.sa

Abstract: This paper proposes a control technique for a large-scale grid-connected photovoltaic (PV) plant that maintains the connection of an inverter to the grid voltage under different types of faults, while injecting a reactive power to accommodate the required grid connection. This control strategy is suggested to improve the low-voltage ride-through (LVRT) capability of grid-connected PV power generation plants. A 20 MW solar PV power plant is modeled and simulated using Matlab/Simulink. The power plant is composed of 10 parallel groups of arrays with a power rating of 2 MWp. The solar PV arrays are connected to a medium-voltage side-rated 22 KV to the utility grid. A dynamic analysis of the grid-connected large-scale solar PV power plant is introduced. This analysis is accomplished in order to determine the impact of three-phase short-circuits at the point of common-coupling (PCC), where the solar PV power station is connected to ensure a practical voltage level by injecting active and reactive power. The reactive power support allows for faster restoration of voltage values at the PCC. When subjected to transient disturbances, the stability of the studied system relies on both the type of the disturbance and the initial operating situation. The disturbance may be either small, resulting from electrical load changes, or large, such as from a transmission line short-circuit (fault) and significant generator loss.

Keywords: dynamic analyses; grid-connected; large-scale PV power plants; voltage source inverter; LVRT capability; reactive power; voltage support requirements

check for updates

Citation: Alrumayh, O.; Sayed, K.; Almutairi, A. LVRT and Reactive Power/Voltage Support of Utility-Scale PV Power Plants during Disturbance Conditions. *Energies* **2023**, *16*, 3245. https://doi.org/10.3390/en16073245

Academic Editor: Abdelali El Aroudi

Received: 14 February 2023
Revised: 28 March 2023
Accepted: 3 April 2023
Published: 5 April 2023

Copyright: © 2023 by the authors. Licensee MDPI, Basel, Switzerland. This article is an open access article distributed under the terms and conditions of the Creative Commons Attribution (CC BY) license (https://creativecommons.org/licenses/by/4.0/).

1. Introduction

Photovoltaic (PV) solar power systems have attracted a great deal of interest recently in several countries, such that a considerable introduction of photovoltaic energy into the power system is anticipated. With a growing interest in PV power generation systems and the adoption of national policies focused on pollution-free energy, an increase in the number of utility-scale-sized PV power plants, which will have a substantial influence on the existing power grid, is expected. PV generation units behave in a different way from conventional generating units, such as thermal, in terms of both their output reactive power capabilities and their fault-ride-through (FRT) capabilities. FRT means the system's aptitude to stay connected and to deliver energy to the electrical network instantaneously after a fault in the network. The control possibilities for distributed power generation systems (DPGS) operating on unbalanced grid faults have been investigated [1]. The investigated control approaches for a grid-side converter can be used for different DPGSs. Moreover, the DC-link voltage controller can be considered in the presence of a PV system's control strategy. These control techniques can be an add-on countenance to the basic control structures of DPGS [2] in order to simplify the different choices when dealing with grid disturbances. Moreover, the solar PV power system is exceedingly non-linear and operates in a changing environment; loads, PV generator outputs, topologies, and key

operating parameters continuously change. A control strategy has been suggested [3] for a three-phase PV generation unit connected to an electricity distribution network. Two control loops are applied: an inward current-control loop and an outside loop for a DC-link voltage regulator. The former algorithm decouples the dynamics of the photovoltaic generator from a medium voltage distribution network and loads, while the latter scheme maximizes the active power generation and enables the power flow control of the PV power plant. Appropriate feedforward schemes have been suggested for the inner control path (current-control) to make the dynamics of the loop independent from the rest of the proposed system. Further, a feedforward compensation scheme has been suggested for the outer control loop to make the dynamics of the PV system resistant to the PV modules' non-linear characteristics. Modeling guidelines are presented in [4]. PV generator simulation studies have employed a voltage source inverter (VSI) for grid integration. Some PV systems with MW capacities have been integrated into the power system, mainly at sub-transmission medium voltage levels. Moreover, large PV generation is expected to be increasingly connected to medium voltage distribution systems where large loads and locally distributed generators also exist. This is important for studying utility-scale PV systems in terms of their dynamic characteristics, control strategies, and performance improvement, and to develop appropriate simulation models. The modeling of the transient and steady-state performance of PV systems have been explored in references [5,6].

Small-scale grid-connected PV generators are not permitted to take action during power distribution faults and should be isolated during distribution network faults. Since the capacity of PV stations is increasing, it is recommended to maintain the operation of these arrays in both normal operating and disturbance circumstances [7–9]. Two new requirements need to be taken into account. The first requirement is that, during the steady-state situation, the grid support should be regulated by providing reactive power and participating in the voltage control of the network. The second requirement, during a transient situation, is keeping the PV farms connected and injecting current during short-circuits and utility faults. PV power plants should be capable of providing dynamic grid support. Therefore, PV farms should not be isolated from the grid either during or after a fault and should not take extra reactive power except before the faulty period. Consequently, the generation station must continue the connection even if a fault arises. Inverters can directly resupply active power after the fault clearance and contribute to the stabilization of the electrical network. This procedure is known as limited dynamical support, which happens if the voltage falls below the defined value. Dynamic grid-support is crucial to stability and security features because frequent interruptions may impact the equipment's lifetime and create additional instabilities in the grid [10]. However, this function can be enhanced if the PV stations can maintain a connection to the grid for as long as possible [11].

Voltage fluctuations and possible harmonics injections can be alleviated by injecting an exact reactive power through the PV power inverter [12–14] or via nearby controlled reactive power sources. An alteration in the renewable power generation can cause substantial oscillations in the voltage magnitude of the distribution grid. Control approaches for the reactive power are required to fully realize the reactive power capabilities of three-phase PV inverters and mitigate power fluctuations. By allowing the control of voltage fluctuations, these control methods enable the three-phase inverter to generate reactive power instead of real power when there are considerable fluctuations. The capacity of the solar PV plant influences the power output fluctuations caused by intermittent cloudiness. It is known that increasing the size of the PV plant leads to a smoothing-out of the output power fluctuations [15–18], which also means that, as the rate of the PV power generation system increases, the PV-grid-connected power system becomes more stable. However, the output variation of the PV system depends on the faults and transiency of the power system [19–21].

To ensure the stability of the power supply, the common requirements are LVRT capability and active/reactive power constraints during and after the fault, as well as the

absorbtion or supply of a reactive current to support the point of common coupling (PCC) after the recovery period and frequency deviation [22–24]. FRT is expressed by a time versus voltage relationship, indicating the minimum possible requirements of the PV farm regarding voltage dip according to the grid code requirements [25–30]. Figure 1 illustrates the typical boundary curve for FRT. This curve is only an example and is different in almost every country.

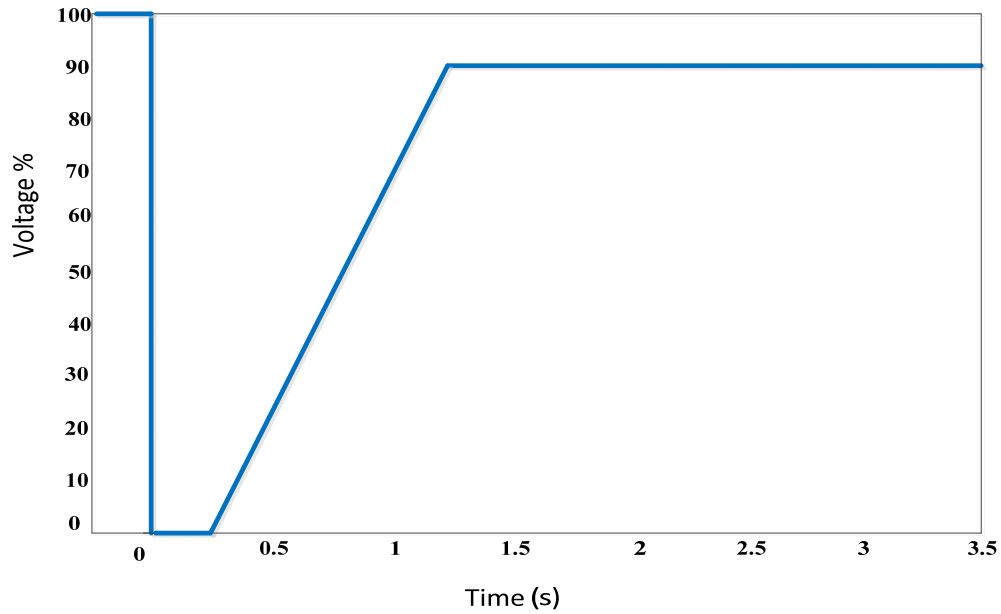

Figure 1. Typical limit curve for FRT requirements.

The active current can be reduced during faults to satisfy the reactive current requirements after the fault period. A quick return to normal active power generation is necessary to maintain the power balance and frequency stability within the studied grid [31–39]. An appropriate reactive current/power has to be injected/absorbed in a voltage deviation situation, as shown in Figure 1. In this case, the slope of the minimum reactive current injection can be in the range of 0–10, while a deadband of 10% voltage deviation is used to improve system stability. The requirements of reactive power production under voltage faults (when V < 0.85 p.u.) are employed in the form of a proportional–integral (PI) voltage controller with a reactive current reference.

This paper examines the dynamic performance of a utility-scale PV plant in the case of unstable conditions resulting from a fault occurrence in the grid. Moreover, it examines the effects of large-scale PV systems' fault ride-through (FRT) capability and dynamic reactive power assistance. The coordinated reactive power control for medium-voltage-distribution grid regulation with PV generation is studied in this article. This study aims to support the grid with reactive power and control the PV system's bus voltage. Therefore, the results obtained from the analysis will enable the flexible design of the active power controller, which can be adjusted to the fault situation. The modeling and control of PV power plant systems are presented, including the modeling of a large-scale PV and the power conditioner unit that interfaces the PV plant to the utility grid with an appropriate control of power flow. The real power output of the PV is given to the switching VSI interfacing with the power grid. The dynamic performance of a large-scale PV generation system is investigated in this paper in the presence of unbalanced conditions caused by utility-grid faults. A flexible active power controller, which can adapt itself to the fault, can be designed based on the results obtained from the system. The PV output is fed to the VSI to interface with the utility grid. Simulations are then conducted to demonstrate the operation principle of the proposed control method.

2. Studied PV Power Plant

Figure 2 represents a schematic block diagram of the proposed 20 MW solar power plant. The diagram contains only a few elements. This PV plant comprises ten PV generators with 2 MVA rated power, a three-phase PWM inverter, and an L filter connected to a 0.4/22 kV transformer. The first winding of each transformer is connected to a low-voltage (LV) bus (700 V). The secondary side of the three-phase transformer is linked to a medium-voltage (MV) bus, which is the connecting point to the PV power plant. The MV bus is connected to the grid and the slack bus through two transmission lines. All the components of the solar PV farm will be explained in detail later in this section. The integration among the different models of 2 MW arrays is presented to construct a large-scale solar PV plant with a rating of 20 MW. Therefore, the control system for the ten parallel inverters is similar. The MV bus of the PV farm is rated 22 kV nominal voltage, and is connected to the PV plant via distribution lines. (In Figure 2, these lines are shown as lines 1–10). The 22 kV bus is connected to the load through line G1. The load bus is connected to the grid using line G2. To specify the lines, two different kinds of lines have to be dimensioned individually since they carry different currents and powers.

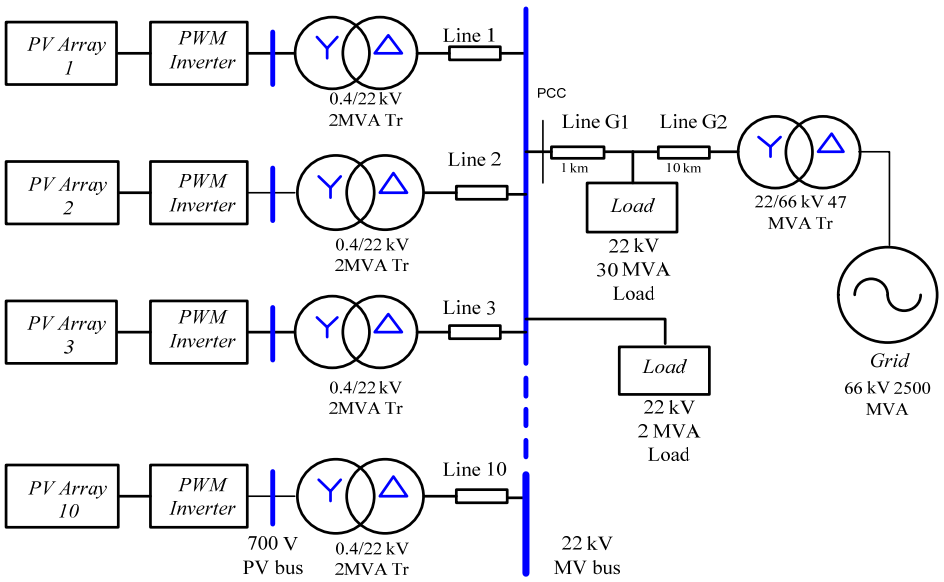

Figure 2. Block diagram of a 20 MW PV power plant.

2.1. PV generators

Figure 2 shows a single-line diagram of the studied three-phase PV power plant interfaced with a medium voltage network at the PCC. The major blocks of the PV schematic are an array of PV panels, a three-phase VSI, and a three-phase interfacing transformer. The PV arrays are in a parallel connection with the DC-link capacitor and input terminals at the DC-side of the VSI. The three-phase VSI is controlled based on the sinusoidal pulse-width-modulation (SPWM) scheme. Each PV generator has a nominal apparent power of 2 MVA. Each PV generation unit is composed of different PV modules to the grid-connection inverter. This PV generator model is called the static model because the PV arrays have no rotating parts, only static ones.

2.2. Voltage Source Inverter

Three-phase VSIs are essential for PV interfacing with the utility grid, as shown in Figure 3. The figure shows a PV-power-inverter-interfacing-grid schematic diagram and the supplementary control strategy. The main aspect is to arrange the inverter's actions to obtain the required power quality for each inverter. Regulating the grid's voltage and sharing the desired active and reactive power are the main requirements for the inverters

according to their ratings. The VSI control strategy should be able to provide flexible operation. If the grid voltage is stiff in the grid-connected systems, voltage regulation of the utility grid might not be required. Therefore, the VSI will perform as a PQ generator and voltage regulation will not be a choice. Conversely, if the stiffness of the utility grid is lower, the DG VSI will support the voltage profile by working as a PV generator. The SPWM modulation strategy would guarantee the minimization of lower-order harmonics in a three-phase VSI inverter current to follow the power quality standards for connecting VSI inverters to the utility grid [23–27]. This function can be accomplished by using the AC-side filter of the VSI.

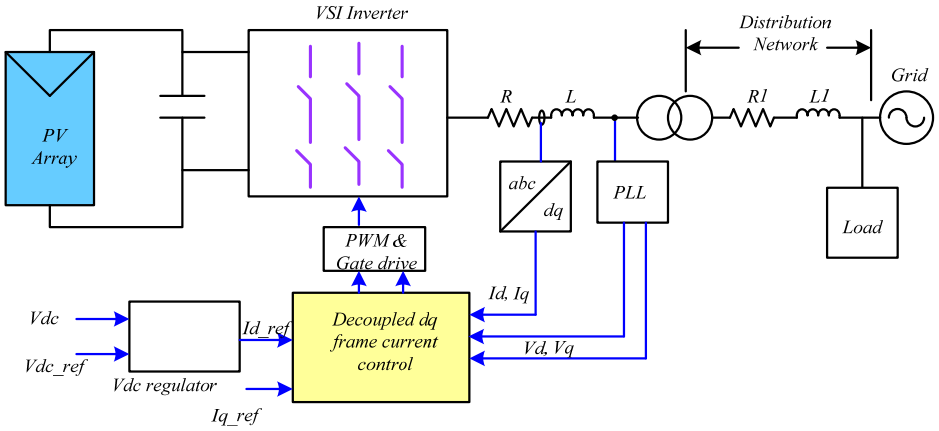

Figure 3. Schematic diagram of voltage-controlled grid-connection inverter.

2.3. Step-Up Transformers

In order to step up the voltage level, 10 units of step-up three-phase transformers are utilized. The power capacity of each transformer is 2 MVA with a rated frequency of 50 Hz. The voltage ratio is 0.4/22 kV. Copper losses are neglected, while the short-circuit voltage is 6%. The transformer has a D1/Yg connection and three single-phase transformers. The medium voltage winding is a solid grounded Y connection. The neutral is held at the zero potential. Therefore, the voltage of the healthy phase under fault in any of the phases remains constant and thus no arcing voltage or over-voltage conditions occur. Solid grounding reduces the possibility of over voltages. The voltage of the healthy phases stays the same as before the fault, requiring less equipment insulation and resulting in cost savings.

2.4. Distribution Lines

The distribution lines are specified according to the data in [10] and are shown in Figure 2. In the case of lines 1 through 10, the lines support a nominal current of In = 2 MW/$\sqrt{3}$ × 22 kV = 52.5 A. The length of these lines is 1 km. According to the tables, for a rated voltage of 22 kV, the cross-section area is 95 mm^2. The resistance, capacitance, and inductance per kilo-meter for the positive and negative sequence of this cable segment can be procured from the manufacturer's tables. The values obtained are listed in Table 1.

The line supports a nominal current of In = 20 MW/$\sqrt{3}$ × 22 kV = 525.4 A. The line is designed by considering the worthiest case when the 2 MVA load is disconnected, and the PV panels supply the maximum power. According to [9], for a rated voltage of 22 kV, the cross-section is 240 mm^2. The values for the cross-section area, inductance, resistance, and capacitance per km, as well as the positive and negative-sequence values, can be obtained from these tables. The obtained values are: Rg′ = 0.124 Ω/km, Lg′ = 0.40 mH/km, and Cg′ = 0.20 μF/km. The values for zero sequence are: Rg′0 = 0.995 Ω/km, Lg′0 = 1.61 mH/km, and Cg′0 = 0.205 μF/km. The power line length is about 10 km. With these line dimensions, the model for the PV generation station is entirely demonstrated.

Table 1. Distribution line parameters.

Description	Symbol	Value
Resistance of Lines 1–10	R'	0.193 Ω/km
Inductance of Lines 1–10	L'	0.43 mH/km
Line capacitance 1–10	C'	0.17 μF/km
Zero-sequence resistance	$R'0$	0.772 Ω/km
Zero sequence inductance	$L'0$	1.72 mH/km
Zero sequence capacitance	$C'0$	0.175 μF/km

3. Control Strategy for the PV Plant

Figure 4 shows the inverter control scheme for the case of a grid-connection operation. Two control loops are employed to control the inverter. Usually, there is a fast inner control loop, which is applied to control the grid current, and an outer voltage control loop, which is responsible for controlling the DC-link voltage. However, the inner control loop leads to power quality issues such as low total harmonic distortion (THD) and a high power factor, while the voltage control loop draws up the power flow in the studied system. The DC-bus voltage of the VSI is measured and compared to the reference value of the DC bus in order to control the active power throughout the inverter. A PI controller manipulates the resulting voltage error, producing a current reference signal as its output. This control process is accomplished through the well-known rotating dq synchronous frame [7]. A synchronous reference frame control utilizes a reference frame transformation of *abc* to *dq* that transforms the measured current and voltage values into a d-q frame based on the fundamental frequency (Figure 4). A special advantage of this control method is that the processing of voltage and current signals is performed in two coordinated systems. The transformed voltage signal detects the phase and frequency of the utility grid, while the transformed current signal monitors the grid current. Consequently, the control variables become dc values, and filtering and control becomes easier. In this case, when integrated with the PI controllers, this transformation eliminates the steady-state error. The voltage equations in the d-q synchronous reference can be expressed as follows:

$$V_d = V_{sd} - R_f I_d - L_f \frac{dI_d}{dt} + \omega L_f I_q \tag{1}$$

$$0 = V_{sq} - R_f I_q - L_f \frac{dI_q}{dt} - \omega L_f I_d \tag{2}$$

where V_d, V_q, I_d, and I_q are the direct-axis and quadrature-axis components of the three-phase AC voltage and currents. R_f and L_f are the output filter resistance and inductance, respectively, and ω is the angular frequency of the utility grid.

Figure 5 shows that the q-axis voltage controller uses the q-axis current to control the flow of the reactive power, while the DC-link voltage controller uses the d-axis current as the desired value to regulate the flow of the active power between the AC bus and the DC bus. The terms $-Lfid$, $Lfiq$ are inserted in order to decouple the dq axes' dynamics. An enhanced voltage oriented control technique (EVOC) was implemented in the PV grid-connected inverter in order to improve the power flow transfer, dynamics, and transient stability [28–30]. The controller is coordinated with the system to gain much better stability and enhanced operation during a grid fault. The conventional voltage oriented control (VOC) scheme for a PV plant is conducted in a synchronously rotating frame to enable decoupled active and reactive power control, and to improve the PV plant performance due to transients by enhancing the dynamic response. The response time of the reactive power controller is about 30 ms maximum and the current control band can range from −10 to +20% of the nominal current.

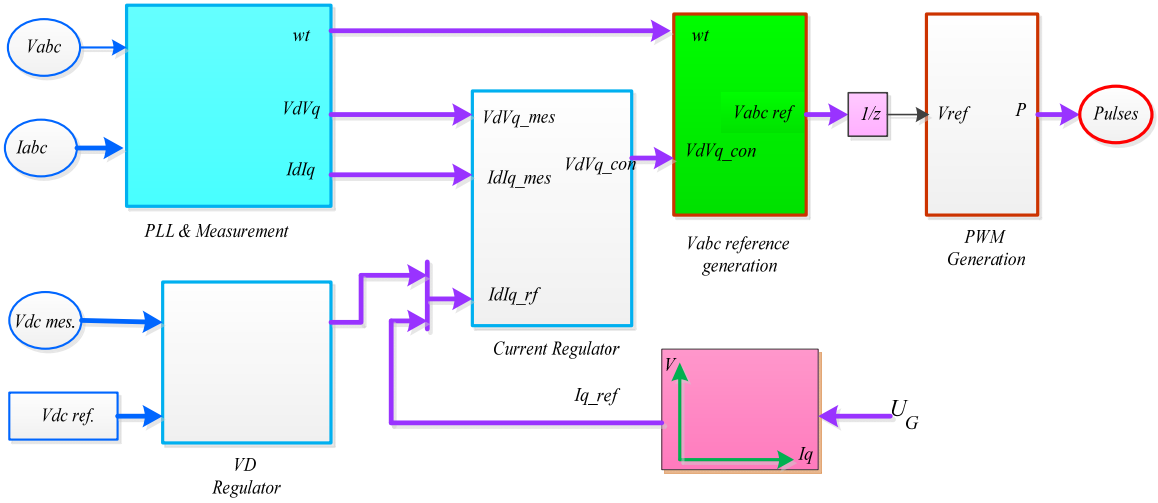

Figure 4. Schematic diagram of the VSI main controller.

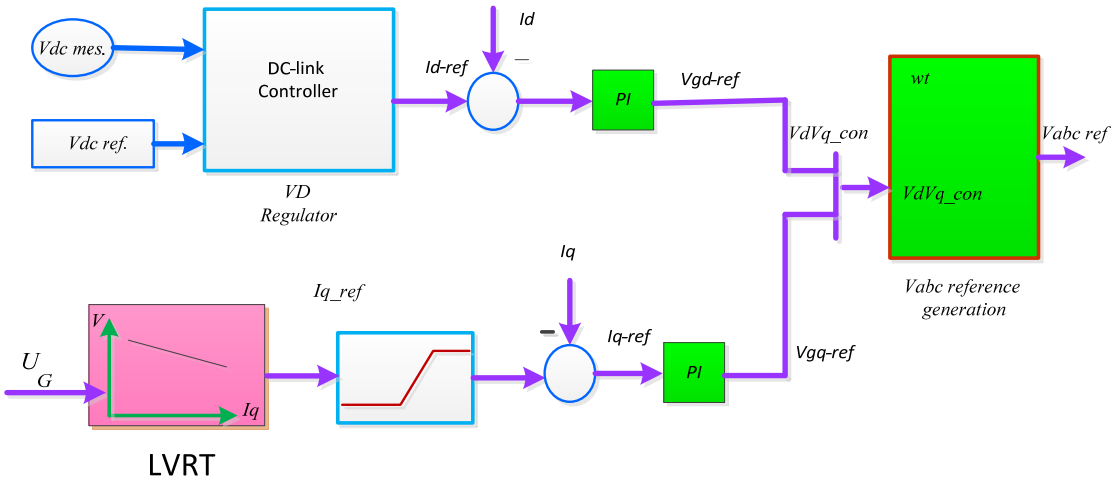

Figure 5. Current regulator using LVRT.

This is developed with the EVOC strategy in order to provide rapid reactive power support to the grid through the d and q axis components of the grid voltage. In order to supply gate pulses for the converter on the grid side, a sinusoidal PWM approach, based on Park's transformation, is used next. Figure 5 shows a schematic of the d-q control. Direct and quadrature current components are applied to control the active and reactive powers, respectively. The DC-bus voltage is truly fed from the PV panels. The reference for active current control is given by the DC-bus voltage, which is supplied by the PV generator. If the reactive power is controlled, the reference settings in the system are used.

A measurement system is utilized to measure the d and q components of the positive-sequence component of the AC voltages and currents to be manipulated, as well as the DC-link voltage, Vdc. A phase-locked loop (PLL) is employed for synchronization with a signal from the three-phase utility voltage. The output signal produced (angle $\theta = \omega t$) is used to determine the direct-axis and quadrature-axis components of the three-phase AC currents and voltages (represented as V_d, V_q or I_d, and I_q).

The outer controller loop is composed of an AC voltage regulation block and a DC-link voltage regulation block. The output signal of the AC voltage regulator is the reference current signal Iqref that is used for regulating the current component in the quadrature axis I_q, which adjusts the reactive power flow. The output of the DC-link voltage regulator is the reference current signal Idref, which is utilized by the current regulator and compared to the I_d component of the current, in phase with the voltage that regulates the flow of active

power. The inner current regulation loop is mainly composed of the current regulator block. The current regulator is used for regulating the magnitude and phase of the AC voltage generated by the voltage source inverter VSI (V_{2d} V_{2q}). The current references Idref and Iqref are produced by the DC-link voltage regulator and the AC voltage regulator, respectively. At the same time, the current regulator is supported by a feed-forward-type regulator, which estimates the output voltage V_2 (V_{2d} V_{2q}) from the measured voltage V_1 (V_{1d} V_{1q}), as well as the transformer leakage inductance.

4. LVRT Conditions

For the period of LVRT, the PV generation plant should be able to connect to the utility grid when the system voltage at the PCC decreases to zero within 0.15 s. Furthermore, the PV power plant cannot be disconnected from the utility grid until the voltage at the PCC is lower than the LVRT line. When a dip occurs, the PV power generation facility must maintain its connection to the grid and must also send reactive power into the grid to help the utility maintain grid voltage. During fault, the PV generation plant should prioritize the supply of a certain amount of reactive power to enable dynamic voltage support. Therefore, the reactive component of the current I_q should agree with the necessities of Equation (3):

$$\begin{cases} I_q \geq 1.5(0.9 - U_G)I_N, & \rightarrow 0.2 \leq U_G \leq 0.9 \\ I_q \geq 1.5I_N, & \rightarrow U_G < 0.2 \\ I_q = 0, & \rightarrow U_G > 0.9 \end{cases} \quad (3)$$

where U_G is the voltage at the PCC (in per unit), and I_N is the rated current of the PV power generator. The active and reactive current components also have to satisfy the subsequent condition

$$I_d^2 + I_q^2 \leq I_{\max}^2 \quad (4)$$

where $I'_{\max}$ is the maximum value of current that the PV generator is allowed to deliver, typically 1.1 times the current rating.

Therefore, the PV inverter can maintain a constant peak value of injection current during LVRT operation to strictly avoid an inverter overcurrent trip. This limit ensures that the inverter is not in danger of overcurrent tripping during LVRT operation. However, the above limitations should be considered during the design and operation phases of PV inverters. The voltage range that the PV inverter can withstand during LVRT is severely limited if a constant power control strategy is employed when the derating operation is disabled. Nevertheless, by using the above reactive power control strategy, both the active and reactive power (depending on the requirement) can be controlled by the LVRT operation.

5. System Simulation

To ensure that the model operates correctly and that the predicted values of both active and reactive powers are provided, simulation results were obtained. The Matlab/Simulink model of the studied plant is displayed in Figure 6. As previously mentioned, this model for 20 MW PV power plants was built up and connected to the power grid. This plant is composed of 10 groups of PV arrays. Each group is rated at 2 MWp which is connected to the power grid using a three-phase inverter and a step-up transformer. The inverter is modular and consists of a number of parallel units. The inverter rating is 2 MW. The power capacity of each transformer is 2 MVA with a rated frequency of 50 Hz and the voltage ratio is 0.4/22 kV. Simulations are carried out to obtain the active and reactive power outputs that are delivered to the grid, as well as the voltage at each point for the ten integrated generators. Table 2 shows the values of the Vdc and the current controller values. Table 3 shows the values of the PV array parameters. The fill factor as a measure of solar PV panel efficiency (FF) is equal to 0.73, according to the data in Table 3.

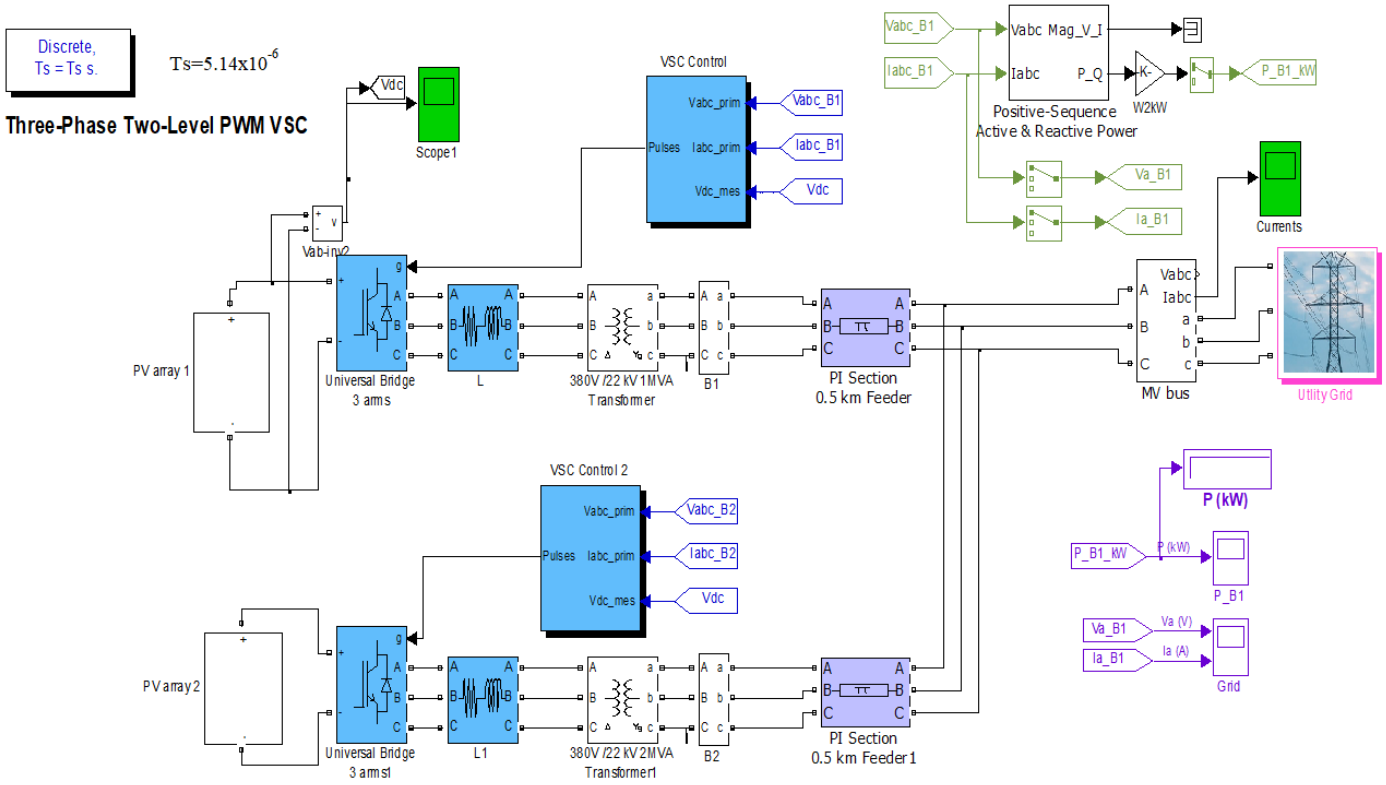

Figure 6. Simulink model of the studied PV plant.

Table 2. Parameters of the controller.

Nominal power P_{nom}	2 MW
Nominal frequency	50 Hz
Initial DC voltage	700 V
Nominal DC voltage U_{dc}	700 V
Rated power P_{nom}	20 MW
Vdc regulator gains K_p and K_i	7 and 800
Current regulator gains K_p and K_i	0.3 and 20
Choke impedance	1 mΩ, 250 µH
Transformer leakage impédance R_xf_o, L_xf / P_{nom}	0.002, 0.06

Table 3. PV array parameters.

Parameter	Value
Open circuit voltage V_{oc}	64 V
Short-circuit current I_{sc}	5.87 A
MPP voltage V_{mp}	54.7 V
MPP current I_{mp}	5.49 A
Number of parallel modules N_p	445
Number of series modules N_s	15

6. Results and Discussion

6.1. Three-Phase-to-Ground Fault at PCC

Simulations were carried out for a three-phase short-circuit at PCC connecting point to illustrate the solar PV farm operation. Each PV generator produces 1.48 MW in normal operating conditions. At these operating condition, the PV generator delivers active power only when the reactive power equals zero ($\cos\varphi = 1$). At the PCC coupling point to the main grid, the solar PV farm injects 1.24 MW and absorbs about 0.125 MVAr, resulting in a power factor $\cos\varphi = 0.9984$. The reactive power is absorbed by the three-phase interfacing transformers. At a steady-state operation, the MV-bus voltage is about 0.9959 p.u., where the voltage at the LV bus is about 0.9944 p.u., and 700 V at the PV bus. In the simulation model, a three-phase short-circuit at the MV bus is simulated and removed after three cycles.

Figure 7a displays the voltage response at the MV bus in kV, Figure 7b displays the MV bus current in amperes, and Figure 7c shows the injected active and reactive power to the grid. No active power is supplied throughout the fault period and a few reactive powers are absorbed due to the presence of the three-phase step-up transformers. The medium voltage winding is a solid-grounded Y connection. The neutral is held at the zero potential. Therefore, the voltage of the healthy phase under fault in any of the phases remains constant, and thus no arcing voltage or over-voltage conditions occur. Solid grounding reduces the possibility of over voltages. The exact values of the voltages and active and reactive powers are noted before and after the time of fault. The DC-link voltage has a maximum value of 876 V because it is determined by the total value of the open-circuit voltage of the PV panels. Figure 8a shows the three-phase voltages at bus 1 while the active and reactive powers of the PV generators injected into the MV bus are shown in Figure 8b. The solar PV generator injects active power at about 2 MW and reactive power at about 1.40 kVAr before and after the fault occurrence. During the fault, an active power of about 0.55 kW is injected into the grid and a reactive power of about 16.2 kVAr is supplied to the grid.

The solar PV farm should be not disconnected when a fault occurs. For this reason, it is necessary to analyze the dynamic network's support. The solar PV generators reach steady-state conditions in a time period equal to 100 ms after the fault at the DC bus, and immediately at the MV and LV buses. During the fault occurrence from 0.4 to 0.5 S, the three-phase voltages in the low-voltage bus during a three-phase-to-ground fault are shown in Figure 9a. The fault currents are shown in Figure 9b. Figure 9c shows the delivered active and reactive powers of one PV generator at the low-voltage bus.

6.2. Single-Phase-to-Ground Fault in the Connection Point

A single-phase-to-ground fault was made in the MV bus. Accordingly, the apparent power due to a short-circuit at the point connected to the external grid is about 450 MVA. At steady-state conditions, the PV farm injects 20 MW into the network and absorbs 0.275 MVAr, which provides a power factor $\cos\theta \approx 1$. This absorption of reactive power is due to the three-phase step-up coupling transformers. Voltages at this condition are 0.9986 p.u. at the MV bus and 700 V at the DC bus for each generator. The short-circuit fault is removed in the simulation after five cycles.

Figure 10 displays the waveforms in the case of a single-phase-to-ground fault. Figure 10c displays the delivered active and reactive powers. Prior to the fault, the solar PV plant supplied 13.46 MW. The PV farm does not inject any active power to the grid during period of fault. The solar PV farm absorbs 0.728 MVAr before and after the fault. During the fault, the PV injects 0.023 MVAr. This agrees with the grid standards for when the solar PV power station has to deliver reactive power for the duration of a fault occurrence. However, the DC-link voltage approximately equals 875 V during the one-phase-to-ground fault, which matches the open-circuit voltage (Voc) of the PV modules.

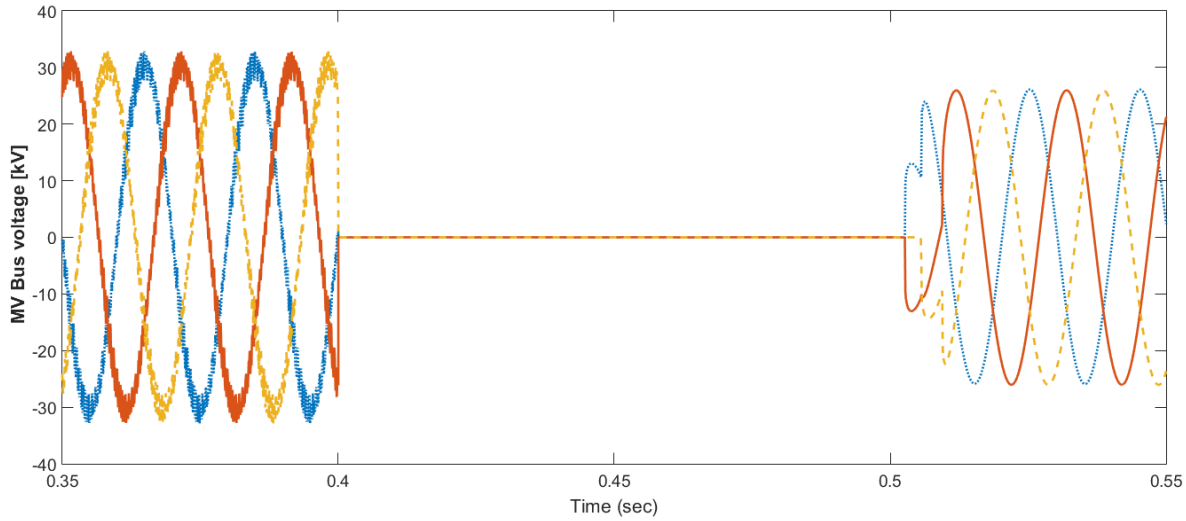

(**a**)

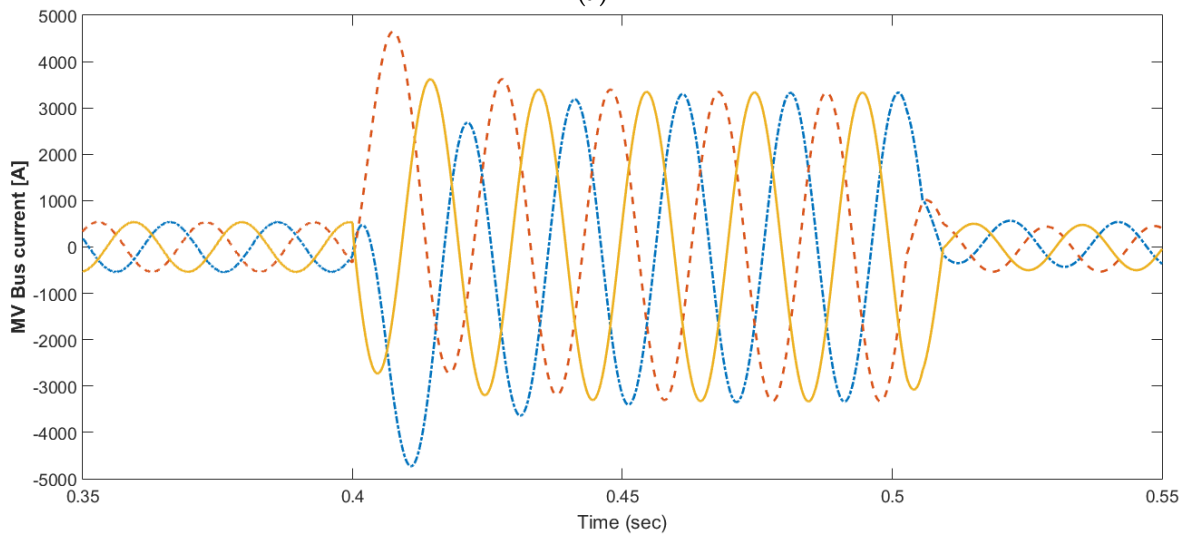

(**b**)

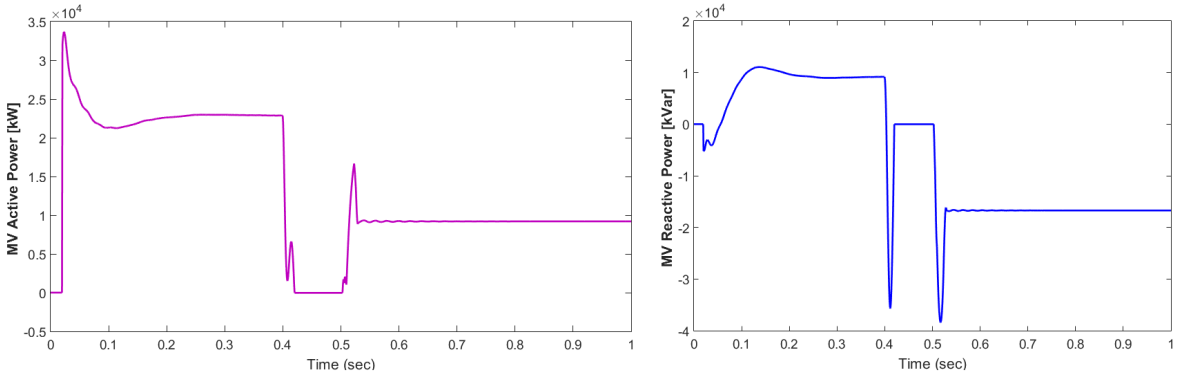

(**c**)

Figure 7. (**a**) Voltage at the MV bus in the case of a three-phase-to-ground fault. (**b**) Currents at the MV bus during a three-phase-to-ground fault. (**c**) Supplied active and reactive powers by each PV generator to the MV bus.

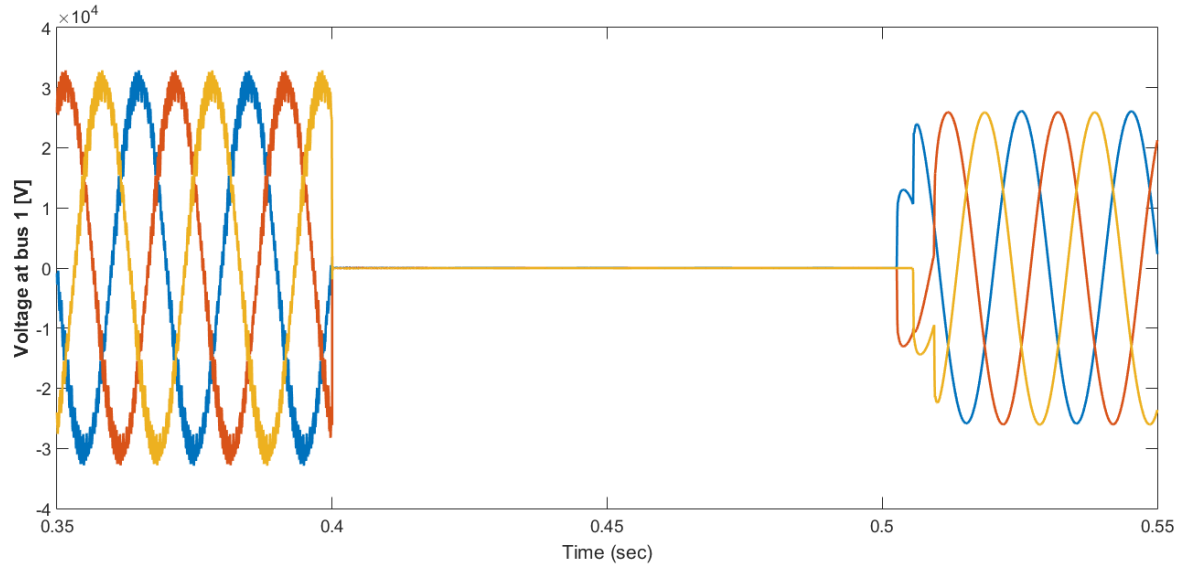

(**a**)

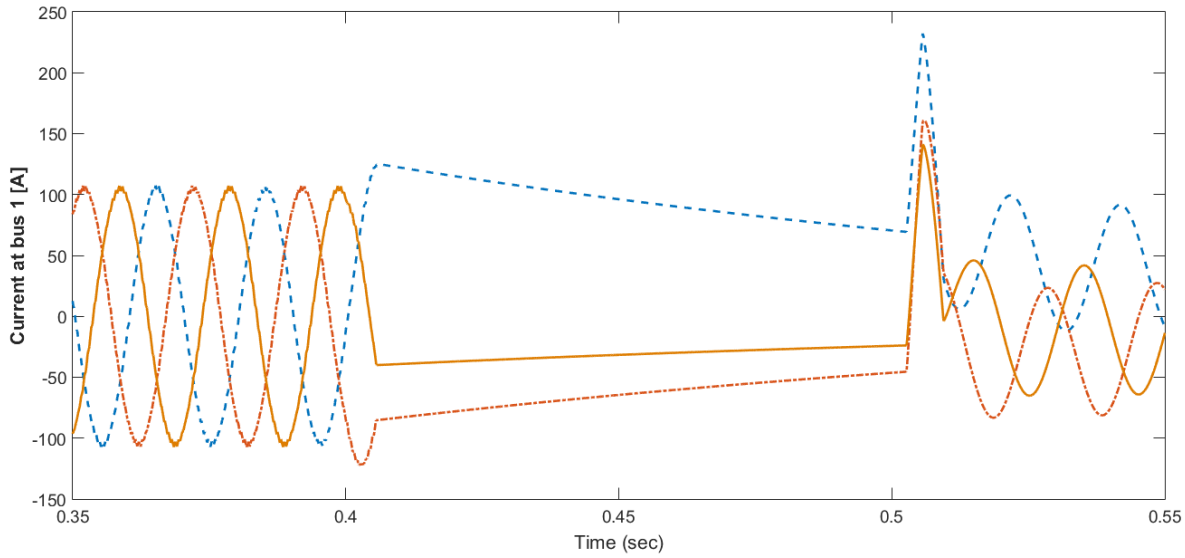

(**b**)

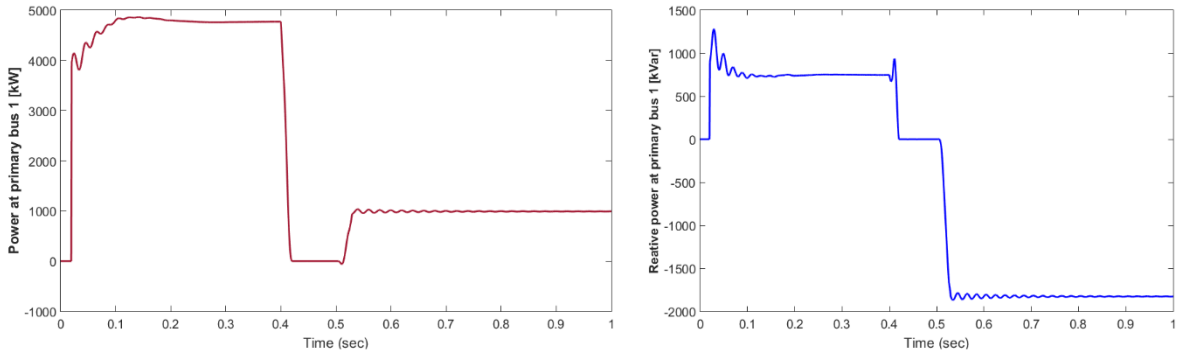

(**c**)

Figure 8. (**a**) Three-phase voltage at bus 1. (**b**). Three-phase current at bus 1. (**c**) Injected active power and (**b**) injected reactive power of one generator.

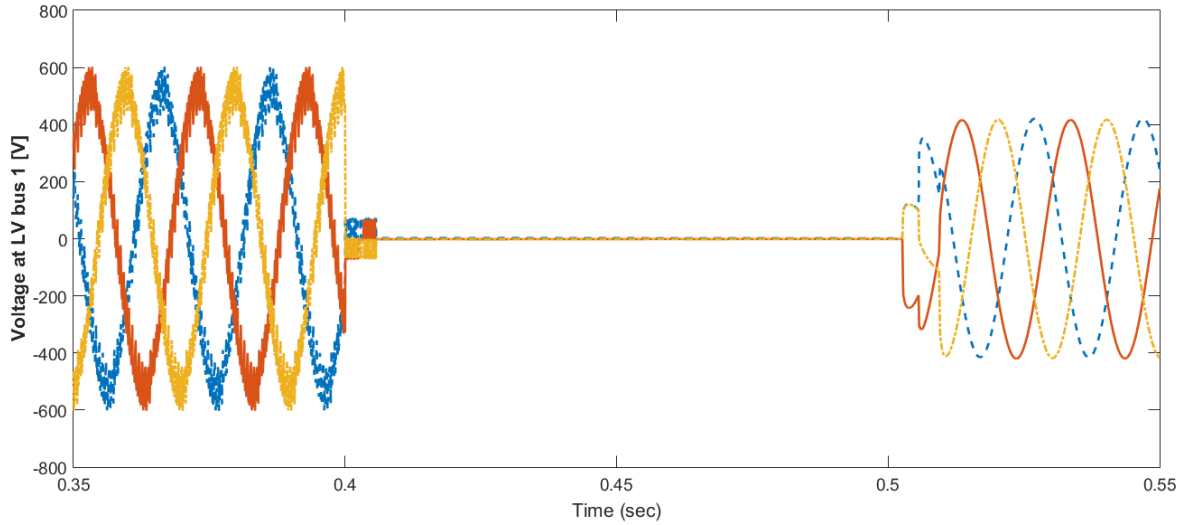

(**a**)

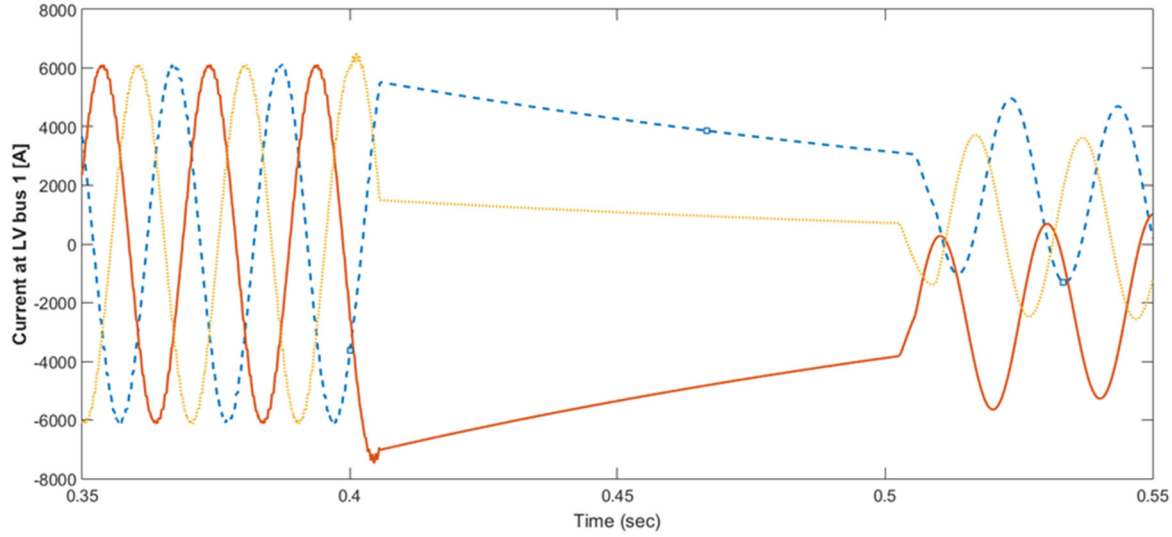

(**b**)

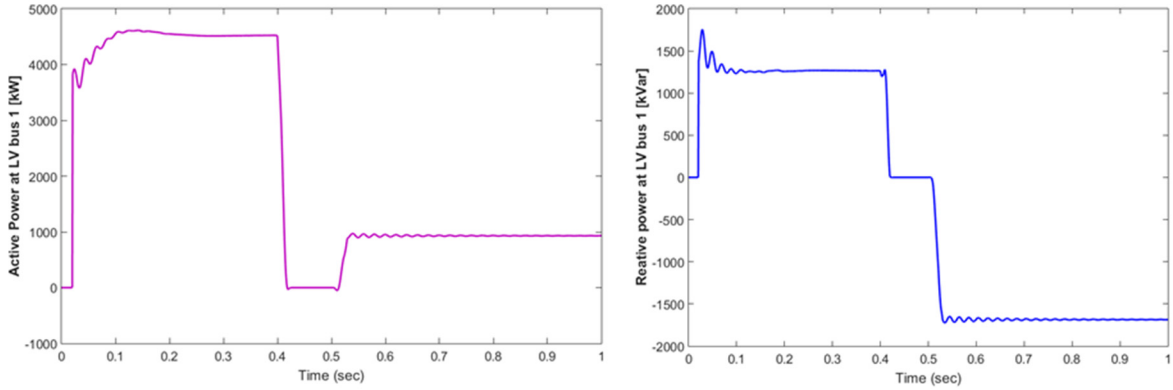

(**c**)

Figure 9. (**a**) Voltage in the low-voltage bus during a three-phase-to-ground fault. (**b**) Three-phase current at the low-voltage bus of one PV generator. (**c**). Supplied active and reactive powers of one PV generator at the low-voltage bus.

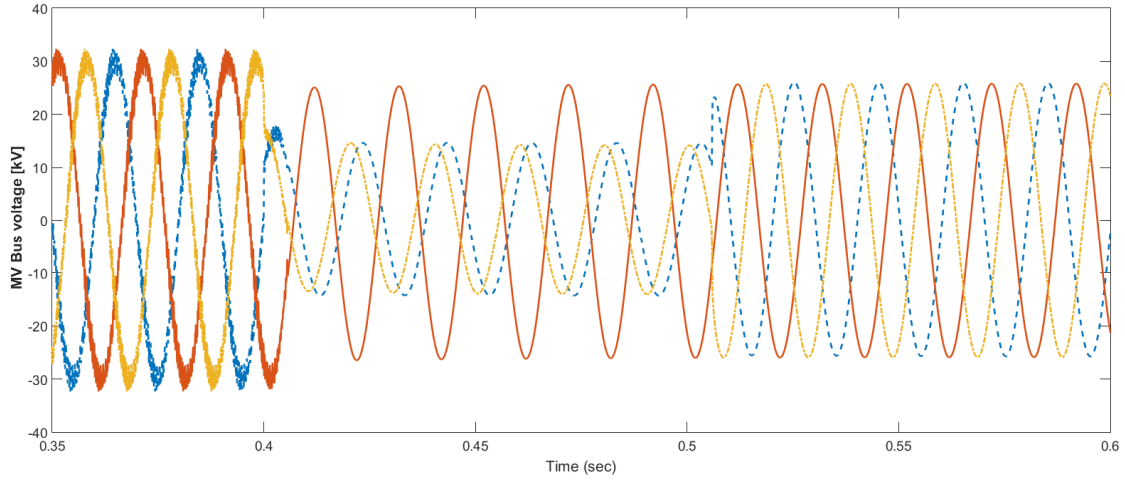

(**a**)

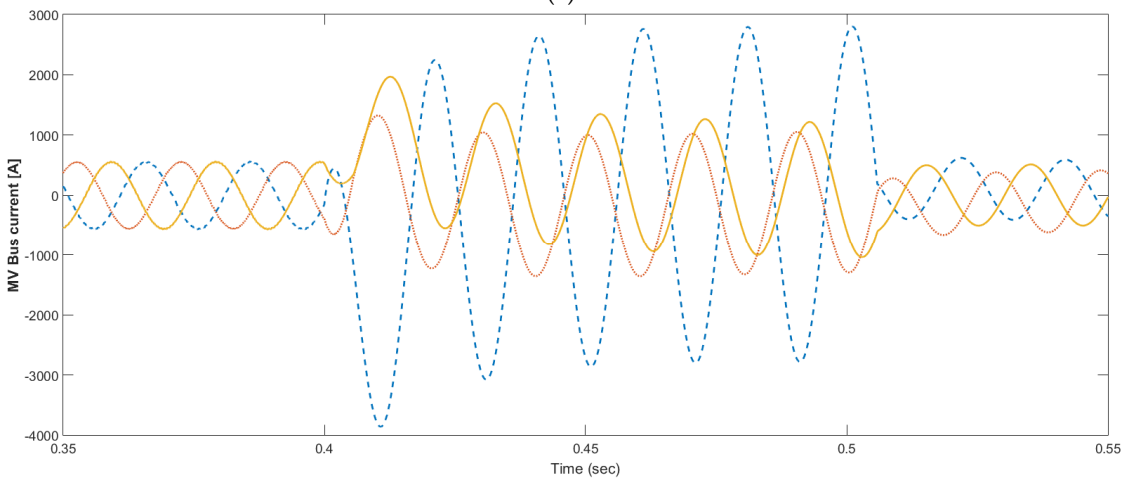

(**b**)

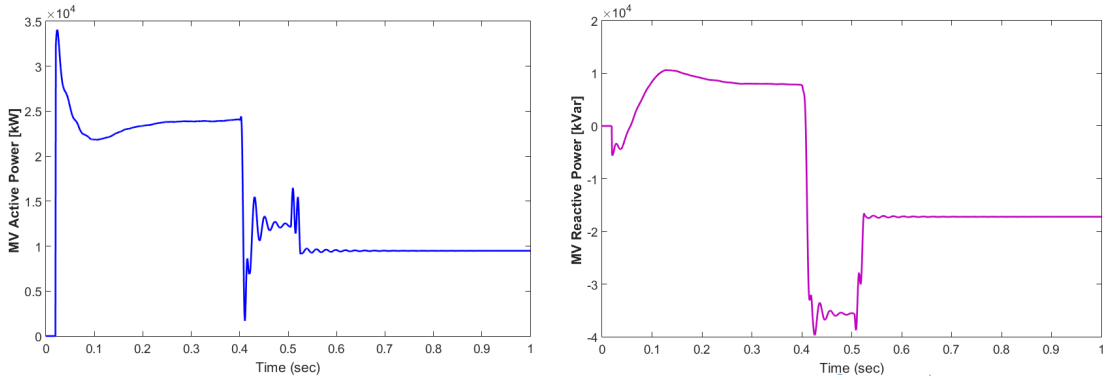

(**c**)

Figure 10. (**a**) Voltages in the MV bus in the case of a one-phase-to-ground fault. (**b**) Currents in the MV park bus in the case of a one-phase-to-ground fault. (**c**) Supplied active and reactive powers of one PV generator at the low-voltage bus during a one-phase-to-ground fault.

Every generator had the same response for both active and reactive powers. The delivered active power both before and after the fault is about 448.9 kW. Throughout the fault period, the generators do not supply any active power. The generation unit absorbs 5.5 kVAr before and after the fault. For the duration of the fault, each generator injects 27.56 kVAr to the utility grid. Figure 11 shows the response of the MV bus's voltage in kV and currents in amperes for the case of the three-phase-to-ground fault. In order to investigate the change in the fault currents and the aggregated contribution, up to 20 MW,

of the distributed PV systems, a fault analysis on the 22 kV line was conducted. Figure 11a shows voltages in the MV park bus in the case of a three-phase-to-ground fault in the 22 kV-side, while the power injected at bus 1 in the case of a one-phase-to-ground fault in the 22 kV-side is shown in Figure 11c.

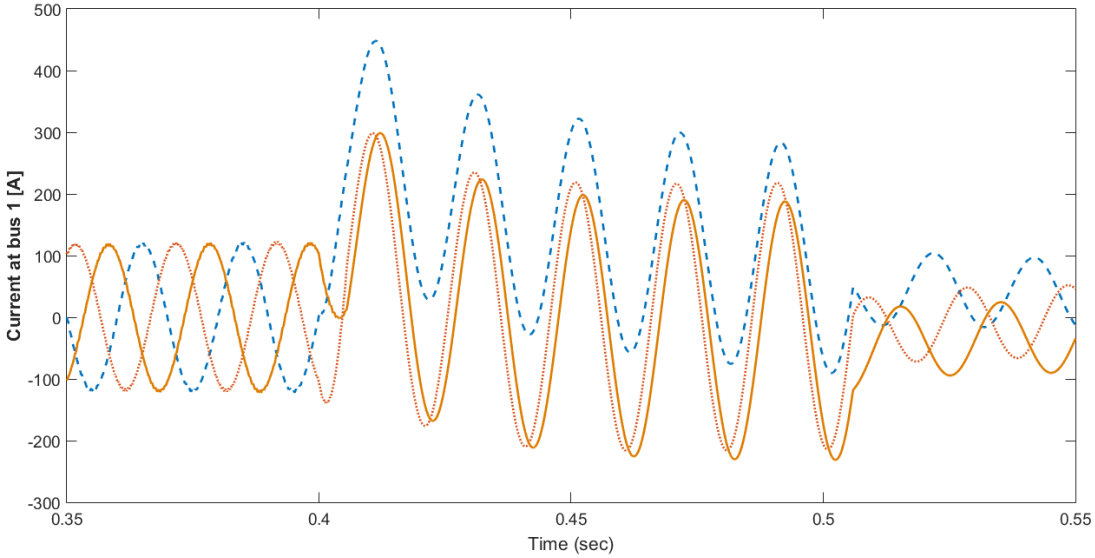

(**a**)

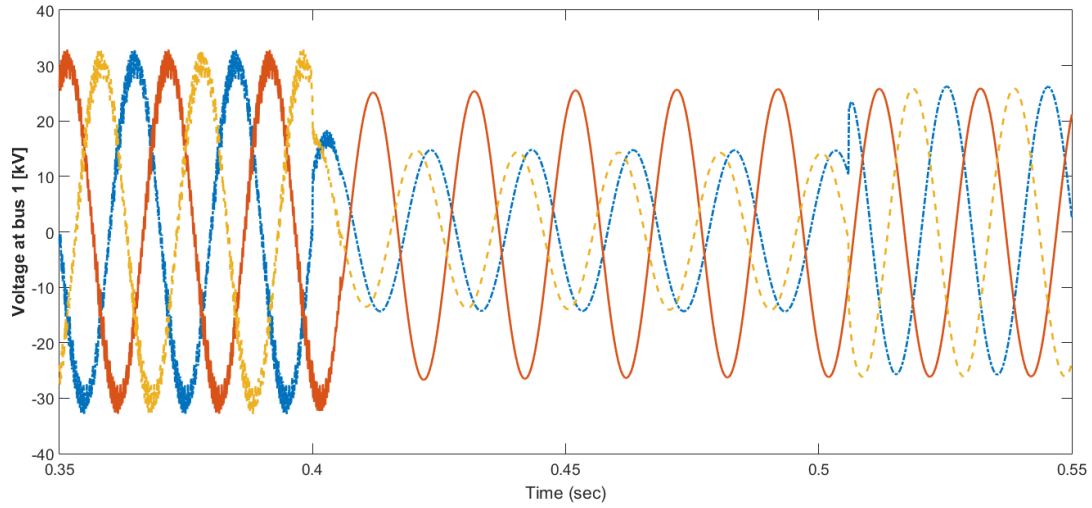

(**b**)

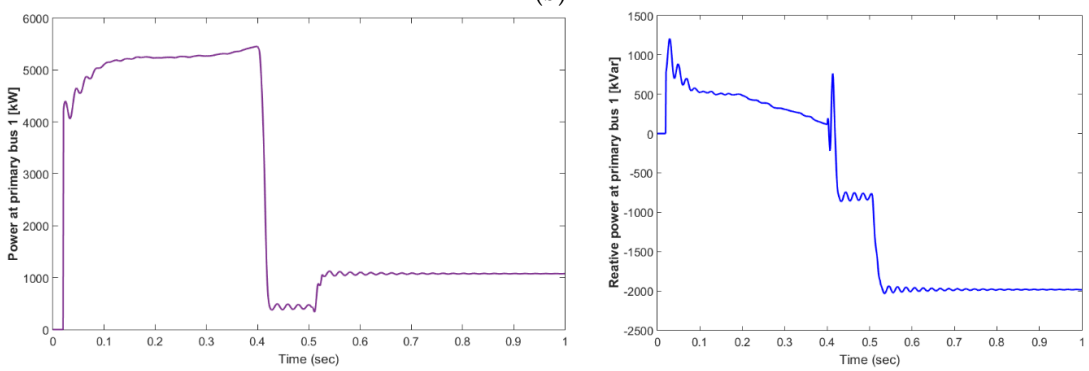

(**c**)

Figure 11. (**a**) Currents in the MV park bus 1 during a three-phase-to-ground fault at the 22 kV-side. (**b**) Voltage at the MV park bus 1 during a three-phase-to-ground fault at the 22 kV-side. (**c**) Active and reactive powers at the MV park bus 1 during a three-phase-to-ground fault at the 22 kV-side.

Figure 12a shows voltages in the LV bus side in the case of a one-phase-to-ground fault in the 22 kV side. Figure 12b shows the currents in the LV bus side in the case of a one-phase-to-ground fault in the 22 kV side. A sensitivity analysis can be conducted by looking at the impact of the PV system faults on the numerous system parameters, including the feeder/line length, X/R ratios, transformer impedance, and system ratings. Figure 12c shows the supplied active power and reactive power of one generator at the low-voltage bus. The severe peak of the inverter current can destroy the inverter power semiconductor devices, except when they are sized to resist grid faults. In order to preclude this appreciated solution, the control of the VSI must be adjusted to obtain better action during grid faults.

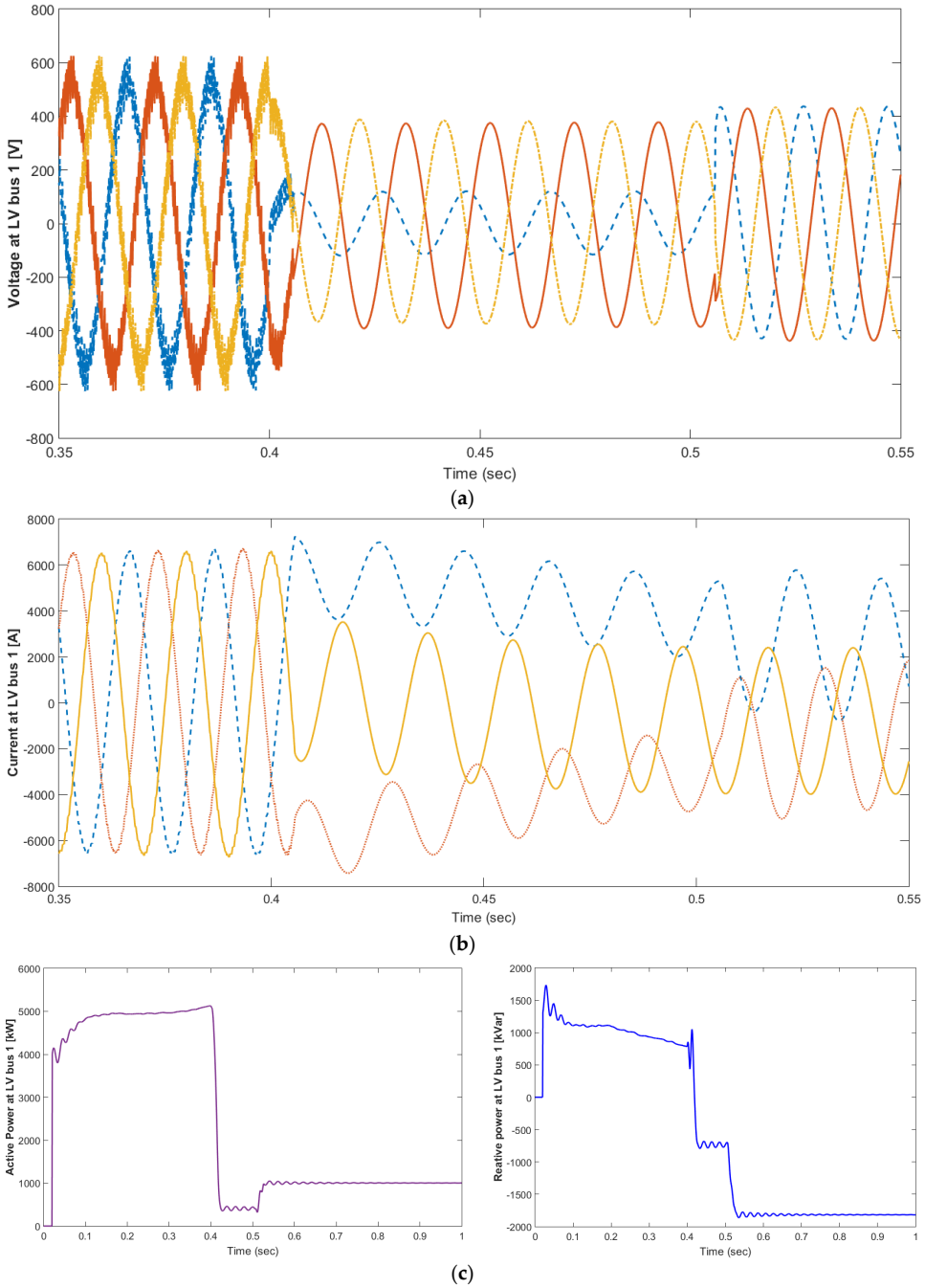

Figure 12. (**a**). Voltages in the LV park bus during one-phase-to-ground fault at the 22 kV side. (**b**) Currents in the LV park bus during one-phase-to-ground fault at the 22 kV side. (**c**). Active and reactive power at the LV bus during one-phase-to-ground fault.

6.3. Active and Reactive Power Response

Solar irradiance is taken to be 1000 W/m^2 in this simulation. Looking at the LVRT, the response waveforms of the active and reactive powers, voltages, and currents at the PCCs are depicted during the three-phase fault period in Figures 13 and 14, respectively. Under these conditions, the voltage at the PCC falls to about 0.20 p.u. The control mode is a LVRT mode to produce a specified amount of reactive power to the utility network. Due to the presence of the reactive current component, the total current at the PCC is more than the regular current. During the period of recovery, there is a linear recovery progression between the active power and the current, which meets the conditions of Equations (3) and (4). This case fruitfully confirms that the simulation model of the PV plant meets the LVRT requirements considered above.

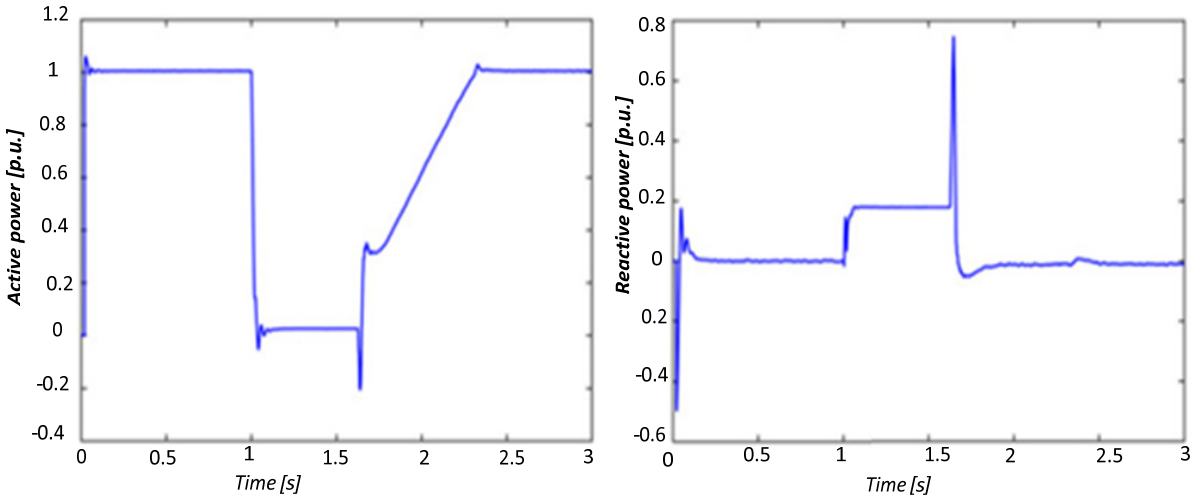

Figure 13. Active and reactive power responses in the case of a three-phase short-circuit.

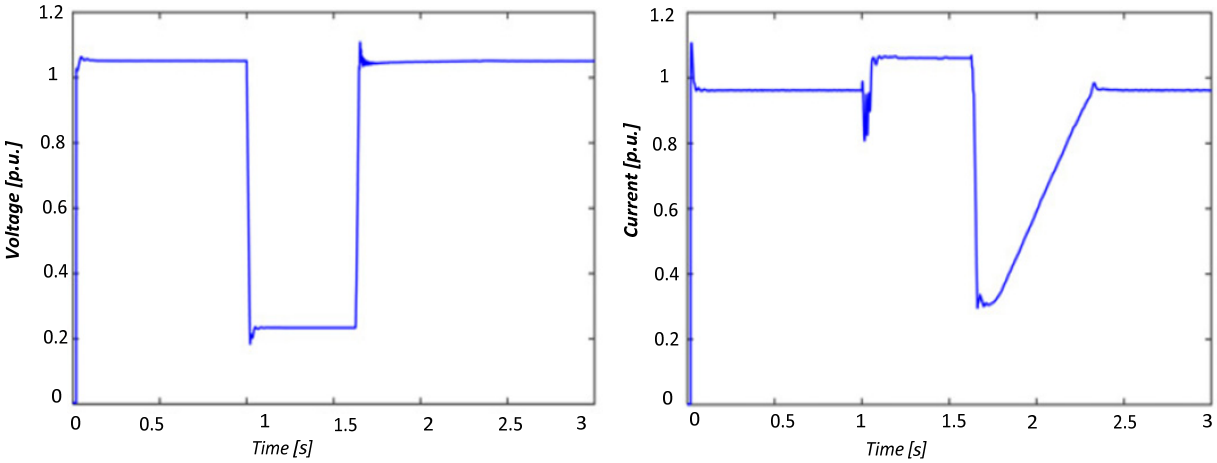

Figure 14. Voltage and current behavior under a three-phase short-circuit.

A transformer enables one to raise the output power of the inverter by introducing active power measurements during significant perturbations and at the site of common coupling. The grid-connected PV-VSI controllers improve inverter performance and distribute reactive power equally. The PV power plant should be able to regulate the reactive power in order to address the issue of a voltage limit brought about by various disturbances. In order to maintain grid voltage, the control strategy coordinates the reactive power compensation device and the inverter's reactive capacity, uses the PI controller to accomplish voltage-free control, and optimizes the inverter's reactive power distribution based on the reactive line loss.

7. Conclusions

LVRT capability and the reactive power/voltage support of a large-scale PV system are introduced in this paper. An advanced simulation tool to conduct a switching transient analysis, Matlab/Simulink, was used to demonstrate the control concept of a large-scale PV system and the impact on the power system. A Simulink-based model of a three-phase grid-connected 20 MW solar PV power plant is presented. This model is composed of 10 units of parallel inverters which work together and share active and reactive power equally. A comparable model is created and the model parameters are identified. The control approach is also proven effective when irradiation conditions are rapidly changing. The effect of a solar PV generation connection to the utility grid is studied and analyzed. A solar PV plant has no mechanical parts, thus the transience will not be subjected to the inertia of the rotating machines and will be quicker. Therefore, restoration of the PV generation system that injects real and reactive power is faster due to the inverter controller and the characteristics of the solar PV generation system. According to the simulation findings, the control strategy can maintain voltage stability and minimize line loss in PV power plants. The simulation results agree with the expected waveforms and allow a study of the operation of solar PV plants under actual environmental conditions. Enhanced control strategies permit solar power plants to establish a central and reliable electrical energy supply. Dynamic grid support to a PV power plant during faults in a medium-voltage grid is verified.

Author Contributions: Conceptualization, K.S.; Methodology, K.S. and O.A.; Software, K.S.; Validation, K.S.; Formal Analysis, A.A.; Investigation, O.A.; Resources, A.A.; Data Curation, K.S.; Writing Draft, K.S.; Writing—Review and Editing, K.S; Visualization, K.S.; Supervision and Project Administration, A.A. All authors have read and agreed to the published version of the manuscript.

Funding: The authors extend their appreciation to the Deputyship for Research & Innovation, Ministry of Education, Saudi Arabia for funding this research work through the project number (QU-IF-4-4-2-29012). The authors also thank to Qassim University for technical support.

Data Availability Statement: We encourage all authors of articles published in MDPI journals to share their research data.

Conflicts of Interest: The authors declare there are no conflict of interest.

References

1. Rodriguez, P.; Timbus, A.V.; Teodorescu, R.; Liserre, M.; Blaabjerg, F. Flexible Active Power Control of Distributed Power Generation Systems During Grid Faults. *IEEE Trans. Ind. Electron.* **2007**, *54*, 2583–2592. [CrossRef]
2. Blaabjerg, F.; Teodorescu, R.; Liserre, M.; Timbus, A. Overview of control and grid synchronization for distributed power generation systems. *IEEE Trans. Ind. Electron.* **2006**, *53*, 1398–1409. [CrossRef]
3. Yazdani, A.; Dash, P.P. A control methodology and characterization of dynamics for a photovoltaic system interfaced with a distribution system. *IEEE Trans. Power Deliv.* **2009**, *24*, 1538–1551. [CrossRef]
4. Yazdani, A.; Di Fazio, A.R.; Ghoddami, H.; Russo, M.; Kazerani, M.; Jatskevich, J.; Strunz, K.; Leva, S.; Martinez, J.A. Modeling Guidelines and a Benchmark for Power System Simulation Studies of Three-Phase Single-Stage Photovoltaic Systems Task Force on Modeling and Analysis of Electronically-Coupled Distributed Resources. *IEEE Trans. Power Deliv.* **2011**, *26*, 1247–1264. [CrossRef]
5. Dash, P.P.; Kazerani, M. Dynamic Modeling and Performance Analysis of a Grid-Connected Current-Source Inverter-Based Photovoltaic System. *IEEE Trans. Sustain. Ener.* **2011**, *2*, 443–450. [CrossRef]
6. El Moursi, M.S.; Xiao, W.; Kirtley, J.L., Jr. Fault ride through capability for grid interfacing large scale PV power plants. *IET Gener. Transm. Distrib.* **2013**, *7*, 1027–1036. [CrossRef]
7. Prodanovic, M.; Green, T.C. High-Quality Power Generation through Distributed Control of a Power Park Microgrid. *IEEE Trans. Ind. Electron.* **2006**, *53*, 1471–1482. [CrossRef]
8. *WECC Guide for Representation of Photovoltaic Systems in Large-Scale Load Flow Simulations*. WECC Renewable Energy Modeling Task Force. Available online: https://www.wecc.org/Reliability/WECCPVPlantPowerFlowModelingGuide.pdf (accessed on 1 January 2023).
9. Ruiz, A. *System Aspects of Large Scale Implementation of a Photovoltaic Power Plant*; Degree Project in Electric Power Systems: Stockholm, Sweden, 2011.

10. Marinopoulos, A.; Papandrea, F.; Reza, M.; Norrga, S.; Spertino, F.; Napoli, R. Grid integration aspects of large solar PV installations: LVRT capability and reactive power/voltage support requirements. In Proceedings of the 2011 IEEE Trondheim PowerTech, Trondheim, Norway, 19–23 June 2011; pp. 1–8.
11. R., U.; D., S. Fault Ride Through in Grid Integrated Hybrid System Using FACTS Device and Electric Vehicle Charging Station. *Energies* **2021**, *14*, 3828. [CrossRef]
12. Wang, S.; Duan, S.; Mi, G.; Lu, Y. Optimized Power Distribution Technology for Fast Frequency Response in Photovoltaic Power Stations. *Energies* **2022**, *15*, 8923. [CrossRef]
13. Sayed, K.; Gabbar, H.A. Smart distribution system Volt/VAR control using the intelligence of smart transformer. In Proceedings of the 2016 IEEE Smart Energy Grid Engineering (SEGE), Oshawa, ON, Canada, 21–24 August 2016; pp. 52–56.
14. Xiao, W.; Dunford, W.G.; Palmer, P.R.; Capel, A. Regulation of photovoltaic voltage. *IEEE Trans. Ind. Electron.* **2007**, *54*, 1365–1374. [CrossRef]
15. Liu, X.; Cramer, A.M.; Liao, Y. Reactive power control methods for photovoltaic inverters to mitigate short-term voltage magnitude fluctuations. *Electr. Power Syst. Res.* **2015**, *127*, 213–220. [CrossRef]
16. Bakirtzis, E.A.; Simoglou, C.K.; Biskas, P.N.; Labridis, D.P.; Bakirtzis, A.G. Comparison of advanced power system operations models for large-scale renewable integration. *Electr. Power Syst. Res.* **2015**, *128*, 90–99. [CrossRef]
17. Craciun, B.-I.; Kerekes, T.; Séra, D.; Teodorescu, R. Frequency Support Functions in Large PV Power Plants With Active Power Reserves. *IEEE J. Emerg. Sel. Top. Power Electron* **2014**, *2*, 849–858. [CrossRef]
18. Marcos, J.; Marroyo, L.; Lorenzo, E.; Alvira, D.; Izco, E. Power output fluctuations in large scale PV plants: One year observations with one second resolution and a derived analytic model. *Prog. Photovolt Res. Appl.* **2011**, *19*, 218–227. [CrossRef]
19. Aly, M.M.; Abdelkarim, E.; Abdel-Akher, M. Mitigation of photovoltaic power generation fluctuations using plug-in hybrid electric vehicles storage batteries. *Int. Trans. Electr. Ener. Syst.* **2015**, *25*, 3720–3737. [CrossRef]
20. Brenna, M.; Foiadelli, F.; Riva, S.; Sapienza, G.; Zaninelli, D. Dynamic model of a storage system with real-time simulation for power system reliability. *Int. Trans. Electr. Ener. Syst.* **2015**, *25*, 3109–3121. [CrossRef]
21. Cheng, J.; Xue, Y.; Guan, M.; Wang, C. Analysis of the commutation failure of inverters during open-conductor faults at the AC side. *Int. Trans. Electr. Ener. Syst.* **2015**, *25*, 1570–1589. [CrossRef]
22. Meyer, R.; Zlotnik, A.; Mertens, A. Fault Ride-Through Control of Medium-Voltage Converters with LCL Filter in Distributed Generation Systems. *IEEE Trans. Ind. Applic.* **2014**, *50*, 5. [CrossRef]
23. *IEEE Standard 1547-2003*; IEEE Standard for Interconnecting Distributed Resources with Electric Power Systems. IEEE: Piscataway, NJ, USA, 2003.
24. *IEEE Standard 929-2000*; IEEE Recommended Practice for Utility Interface of Photovoltaic (PV) Systems. IEEE: Piscataway, NJ, USA, 2000.
25. Sayed, K.; Abdel-Salam, M. Dynamic performance of wind turbine conversion system using PMSG-based wind simulator. *Electr. Eng. J.* **2017**, *99*, 431–439. [CrossRef]
26. Balaguer, I.J.; Lei, Q.; Yang, S.; Supatti, U.; Peng, F.Z. Control for Grid-Connected and Intentional Islanding Operations of Distributed Power Generation. *IEEE Trans. Ind. Electron.* **2011**, *58*, 147–157. [CrossRef]
27. Photovoltaic Cell I-V Characterization Theory and LabVIEW Analysis Code—Part II, White Paper, National Instruments, May 2012. Available online: http://www.ni.com/white-paper/7230/en/ (accessed on 1 January 2023).
28. Ananth, D.V.N.; Nagesh Kumar, G.V. Fault ride-through enhancement using an enhanced field oriented control technique for converters of grid connected DFIG and STATCOM for different types of faults. *ISA Trans.* **2016**, *62*, 2–18. [CrossRef] [PubMed]
29. Abdel-Salam, M.; Kamel, R.; Khalaf, M.; Sayed, K. Analysis of overcurrent numerical-relays for protection of a stand-alone PV system. In Proceedings of the 2014 Saudi Arabia Smart Grid Conference (SASG), Jeddah, Saudi Arabia, 14–17 December 2014; pp. 1–6.
30. Abdel-Salam, M.; Kamel, R.; Sayed, K.; Khalaf, M. Design and implementation of a multifunction DSP-based-numerical relay. *Electr. Power Syst. Res.* **2017**, *143*, 32–43. [CrossRef]
31. Abo-Khalil, A.G.; Alyami, S.; Sayed, K.; Alhejji, A. Dynamic Modeling of Wind Turbines Based on Estimated Wind Speed under Turbulent Conditions. *Energies* **2019**, *12*, 1907. [CrossRef]
32. Sayed, K.; Abo-Khalil, A.G.; Alghamdi, A.S. Optimum resilient operation and control dc microgrid based electric vehicles charging station powered by renewable energy sources. *Energies* **2019**, *12*, 4240. [CrossRef]
33. Abo-Khalil, A.G.; Eltamaly, A.M.; Alsaud, M.S.; Sayed, K.; Alghamdi, A.S. Sensorless control for PMSM using model reference adaptive system. *Int. Trans. Electr. Ener. Syst.* **2021**, *31*, e12733. [CrossRef]
34. Eltamaly, A.M.; Al-Saud, M.; Sayed, K.; Abo-Khalil, A.G. Sensorless Active and Reactive Control for DFIG Wind Turbines Using Opposition-Based Learning Technique. *Sustainability* **2020**, *12*, 3583. [CrossRef]
35. Praveen, R.P.; Therattil, J.; Jose, J.; Abo-Khalil, A.; Alghamdi, A.; Bindu, G.R.; Sayed, K. Hybrid Control of a Multi Area Multi Machine Power System with FACTS Devices using Non-linear Modelling. *IET Gener. Transmi. Distrib.* **2020**, *14*, 1993–2003.
36. Abo-Khalil, A.G.; Alghamdi, A.S.; Eltamaly, A.M.; Al-Saud, M.S.; R.P., P.; Sayed, K.; Bindu, G.R.; Tlili, I. Design of State Feedback Current Controller for Fast Synchronization of DFIG in Wind Power Generation Systems. *Energies* **2019**, *12*, 2427. [CrossRef]
37. Hasanien, H.M. An Adaptive Control Strategy for Low Voltage Ride Through Capability Enhancement of Grid-Connected Photovoltaic Power Plants. *IEEE Trans. Power Syst.* **2016**, *31*, 3230–3237. [CrossRef]

38. Sakib, M.N.; Azad, S.P.; Kazerani, M. A Critical Review of Modular Multilevel Converter. *Energy Eng.* **2019**, *7*, 62–79.
39. Sayed, K.; Abdel-Khalek, S.; Zakaly, H.M.H.; Aref, M. Energy Management and Control in Multiple Storage Energy Units (Battery–Supercapacitor) of Fuel Cell Electric Vehicles. *Materials* **2022**, *15*, 8932. [CrossRef] [PubMed]

Disclaimer/Publisher's Note: The statements, opinions and data contained in all publications are solely those of the individual author(s) and contributor(s) and not of MDPI and/or the editor(s). MDPI and/or the editor(s) disclaim responsibility for any injury to people or property resulting from any ideas, methods, instructions or products referred to in the content.